pubs.acs.org/cm Article

Site Occupation Engineering toward Giant Red-Shifted Photoluminescence in (Ba,Sr)$_2$LaGaO$_5$:Eu^{2+} Phosphors

Yu Chen, Zhiyu Yang, Jiance Jin, Jianwei Qiao, Yuzhen Wang, Maxim S. Molokeev, Hendrik C. Swart, and Zhiguo Xia*

Cite This: Chem. Mater. 2023, 35, 8714−8721 Read Online

ACCESS | Metrics & More | Article Recommendations | Supporting Information

ABSTRACT: Exploring oxide-based red-emitting phosphors is essential for improving the color rendering index (R_a) and reducing the correlated color temperature (CCT) of white-light-emitting diode (LED) lighting sources. Especially, it is challenging to design Eu^{2+} red emission in inorganic solids. Here, the Eu^{2+}-activated oxide phosphor Sr$_2$LaGaO$_5$:Eu^{2+} was synthesized with red emission peaking at 618 nm under 450 nm excitation. The crystal structure and spectral analysis indicate that Eu^{2+} tends to occupy [Sr1/LaO$_8$] polyhedrons with a smaller coordination number, resulting in a large crystal field splitting at the 5*d* level and realizing the broadband 4*f*−5*d* red emission. When Sr is substituted by Ba atoms, density functional theory calculations verify that Ba tends to enter [Sr2O$_{10}$] with a large coordination number, further giving rise to the lattice distortion and a giant spectral redshift (618−800 nm). The white LED device fabricated by mixing red Sr$_{1.8}$Ba$_{0.2}$GaO$_5$:Eu^{2+} and green Lu$_3$Al$_5$O$_{12}$:Ce^{3+} phosphors exhibits a high color rendering index (R_a = 92.1) and a low color-dependent temperature (CCT = 4570 K). This study will give guidance for exploring new Eu^{2+} activated oxide-based red phosphors as well as achieving tunable emission through cations' substitution.

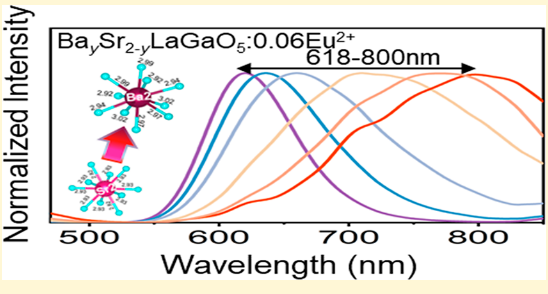

■ INTRODUCTION

Phosphor-converted white-light-emitting diodes (pc-WLEDs) are considered as the new generation of lighting sources owing to their merits involving compact structures, energy conservation, environmental protection, high efficiency, and long service life.[1−4] Therefore, developing pc-WLED lighting will help alleviate the energy crisis, environmental pollution, and other adverse situations. So far, exploring new red-emitting phosphors is still one of the main challenges to solve the problem of high correlated color temperature (CCT > 4500 K) and low color rendering index (R_a < 80) of commercial pc-WLEDs.[5,6] The present commercial red phosphors are confined to nitride, sulfide, and fluoride, such as CaAlSiN$_3$:Eu^{2+},[7] Sr[LiAl$_3$N$_4$]:Eu^{2+},[8] CaS:Eu^{2+},[9] and K$_2$SiF$_6$:Mn^{4+}.[10] However, synthesizing nitride phosphors requires a high temperature, high pressure, and expensive reagents, which increases the preparation cost. The physical and chemical properties of synthesized sulfide phosphors are unstable, and they may also decompose, which is harmful to environments. Fluoride phosphors have the drawback of requiring the use of toxic and corrosive HF as a fluorine source.[11] In contrast, oxide matrixes have some advantages, including adjustable structure, low cost, and no pollution. Especially, it is significant to explore Eu^{2+} doped red phosphors in the oxide-based inorganic solids because they can be excited by cheap and efficient blue GaN chips. In recent years, some reported Eu^{2+} doped oxide phosphors with red emissions also encourage research in this field.[12]

The local environment around Eu^{2+} ions plays an essential role in photoluminescence tuning. In general, tunable emissions in a given Eu^{2+} activated inorganic phosphor can be achieved by adjusting the local environment around the Eu^{2+} ion. For example, as the Sr content gradually increases in Sr$_x$Ba$_{2-x}$SiO$_4$:Eu^{2+}, the Eu−O bond length decreases correspondingly, leading to tunable emission colors from green to orange red.[13] In addition, the local environment of Eu^{2+} in Sr$_{1-x}$Ba$_x$Y$_2$O$_4$:Eu^{2+} can also be modified through Sr/Ba substitution to achieve spectral regulations, leading to a substantial red shift emission from 620 to 773 nm.[14] Accordingly, the cation substitution is promising to achieve spectral regulation.

In this work, we designed the synthesis of red-emitting Sr$_2$LaGaO$_5$:Eu^{2+} phosphors with good thermal stability. Eu^{2+} ions preferentially occupy [Sr1/LaO$_8$] polyhedrons with small coordination numbers causing large crystal-field splitting (ε_{CFS}) of 5*d* levels of Eu^{2+}. Through Sr/Ba substitution, the

Received: August 8, 2023
Revised: September 21, 2023
Published: October 5, 2023

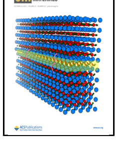

https://doi.org/10.1021/acs.chemmater.3c01980
Chem. Mater. 2023, 35, 8714−8721

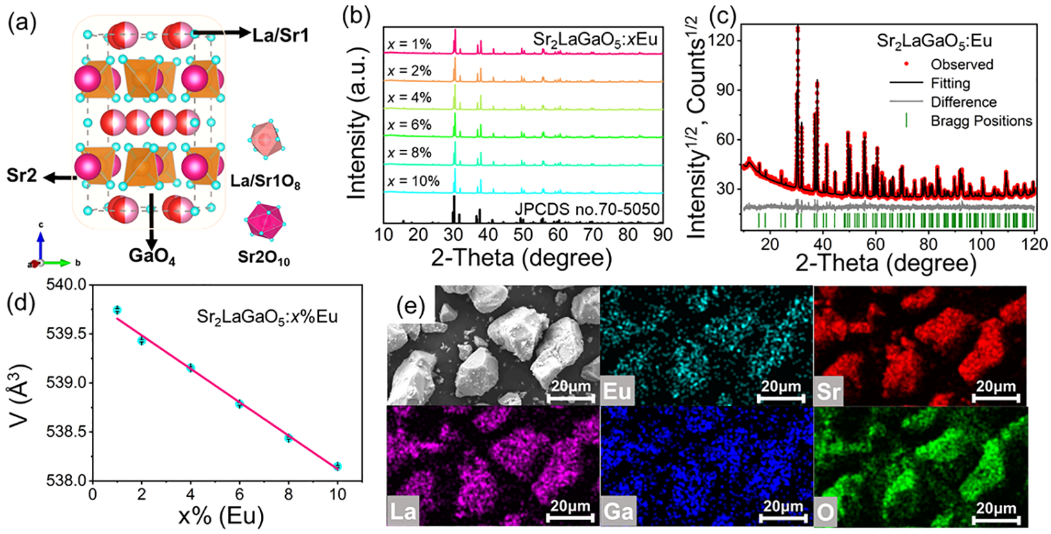

Figure 1. (a) Crystal structure of Sr_2LaGaO_5 highlighting the coordination numbers of each different cation. (b) XRD patterns of Sr_2LaGaO_5:$x$$Eu^{2+}$ ($0.01 \leq x \leq 0.1$). (c) Rietveld refinement of the selected sample of Sr_2LaGaO_5:0.06Eu^{2+}. (d) The relationship between cell volume V (x) and x (Eu) concentration in Sr_2LaGaO_5:$x$$Eu^{2+}$ and (e) scanning electron microscopy of Sr_2LaGaO_5:Eu^{2+} particles and electron spectroscopy of Sr, La, Ga, O, and Eu.

emission peak is further tuned to the near-infrared region and $(Ba,Sr)_2LaGaO_5$:Eu^{2+} maintains good thermal stability. The local environment around Eu^{2+} ions and the mechanism for tunable emission through substitution are analyzed in detail. Furthermore, WLEDs are also fabricated to evaluate the performance of $(Ba,Sr)_2LaGaO_5$:Eu^{2+}, demonstrating their high potential in developing solid-state lighting sources.

EXPERIMENTAL SECTION

Materials. $SrCO_3$ (99.95%, Aladdin), $BaCO_3$ (99.95%, Aladdin), La_2O_3 (99.99%, Aladdin), Ga_2O_3 (99.99%, Aladdin), and Eu_2O_3 (99.99%, Sinopharm). All the reagents were purchased from Aladdin Industrial Corporation and used without additional purification.

Synthesis. Sr_2LaGaO_5:xEu ($0.01 \leq x \leq 0.1$) and $Ba_ySr_{2-y}LaGaO_5$:Eu^{2+} ($0 \leq y \leq 1$) phosphors were synthesized by the high-temperature solid-state method. Based on the above ingredients, the required raw materials were weighed according to their stoichiometric ratios and ground in an agate for approximately 30−40 min for thoroughly mixing. Afterward, the mixture was poured into an alumina crucible, heated to 1450 °C in a horizontal tube furnace under a reducing mixture atmosphere of H_2 (20%) and N_2 (80%), held for 6 h, and then cooled to room temperature. Subsequently, the sample was thoroughly ground again, poured into an alumina crucible, and then sintered again at 1450 °C in a mixed atmosphere of H_2 (20%) and N_2 (80%) for 6 h. After cooling to room temperature, the resultant solid was ground to fine powder for further measurement.

Characterization. An Aeris powder X-ray diffraction (PXRD) diffractometer (PANalytical Corporation, Netherlands) was used to collect the PXRD patterns of all samples under monochromatic Cu Kα radiation (λ = 1.5406 Å) at 40 kV and 15 mA. The morphology and particle size were characterized by using a scanning electron microscope (SEM) (NOVA NANOSEM 430), and the elemental mappings were obtained using an energy dispersive X-ray spectrometer (EDS) attached to the SEM. An FLS1000 fluorescence spectrophotometer from Edinburgh Instruments, equipped with a xenon (Xe) lamp as a radiating source, was used to measure the photoluminescence (PL) and photoluminescence excitation (PLE) spectra, luminescence attenuation curves, and temperature-dependent emission spectra of all samples. Thermoluminescence (TL) spectra were recorded by an FJ427A1 thermoluminescence dosimeter (CNNC Beijing Nuclear Instruments Factory) between 50 and 300 °C at a heating rate of 4 °C s^{-1}. The photoluminescence quantum yield (PLQY) was measured by using an integrated sphere on the same Edinburgh FLS1000 fluorescence spectrophotometer. WLED devices were fabricated by combining the commercial blue InGaN chips with λ_{em} = 450 nm, green-emitting LuAG:Ce^{3+} phosphor, and red-emitting $Ba_{0.2}Sr_{1.8}LaGaO_5$:Eu^{2+} phosphor. The PL spectra R_a, LE, and CCT of the WLEDs were measured by using an integrating sphere spectral Radiometer system (ATA-1000, Ever fine).

COMPUTATIONAL METHODOLOGY

Density functional theory (DFT) calculations were performed for Sr_2LaGaO_5 using the Vienna *Ab initio* Simulation Package (VASP).[15,16] Considering the co-occupied Sr/La atom in one site, six models were first constructed to locate Sr and La at different sites with the formula Sr:La = 2:1. During the calculation, the projector augmented wave (PAW) method based on the generalized gradient approximation (GGA) was employed, and the Perdew−Burke−Ernzerhof (PBE) format was adopted for the exchange correlation potential.[17,18] Structural optimization was conducted by using the PBE exchange correlation potential for each model. The cutoff energy of a plane-wave basis was set as 520 eV. The atoms in each compound were fully relaxed until the Hellmann−Feynman forces on them were within −0.01 eV/Å. The model with the lowest energy formation was chosen for the Ba/Sr substitution. Calculation parameters for the $Ba_ySr_{2-y}LaGaO_5$ were set similarly to those for Sr_2LaGaO_5.

RESULTS AND DISCUSSION

Structural Characterization. As displayed in Figure 1a, Sr_2LaGaO_5 belongs to the $I4/mcm$ space group.[19] Sr has two coordination modes. Sr1 and La are randomly distributed in Sr_2LaGaO_5 with a ratio of 1:1, and they form a eight-coordination polyhedron with oxygen. Sr2 and oxygen form a decacoordinated polyhedron, and Ga and oxygen form a four-coordinated polyhedron. Figure 1b shows that the diffraction peaks of all samples match well with the standard crystallography data, indicating the pure tetragonal phase of Sr_2LaGaO_5 (JCPDS No. 50-0500)[19,20] (Figure 1c, Figure S1, Supporting Information). All fitting parameters R_p, R_{wp}, and χ^2 are presented in Table S1, Supporting Information, and the

https://doi.org/10.1021/acs.chemmater.3c01980
Chem. Mater. 2023, 35, 8714−8721

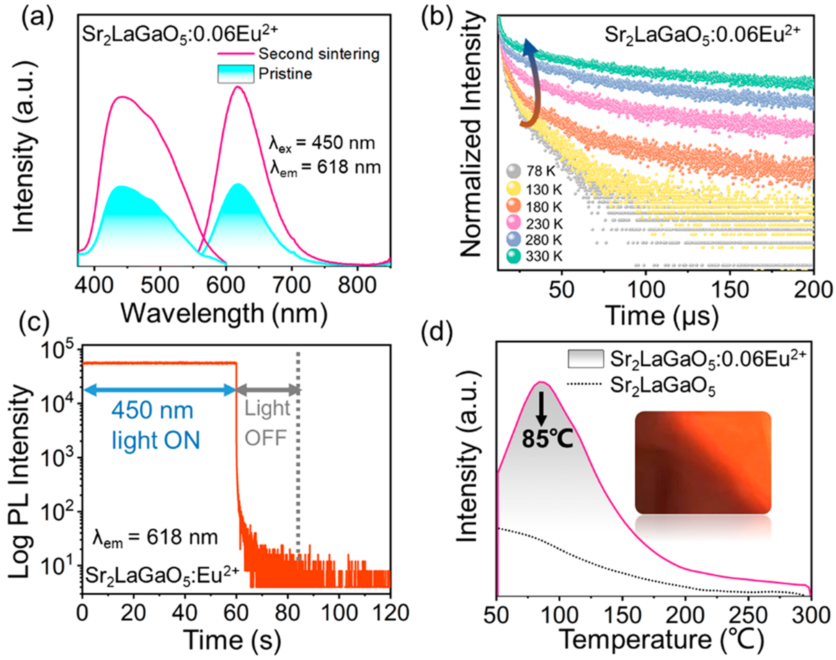

Figure 2. (a) PL emission and excitation spectra of $Sr_2LaGaO_5:Eu^{2+}$ before and after second sintering under 450 nm excitation. (b) Luminescence decay curves of $Sr_2LaGaO_5:0.06Eu^{2+}$ at 78−330 K under excitation at 450 nm and monitored at 618 nm. (c) Persistent luminescence decay curve of $Sr_2LaGaO_5:Eu^{2+}$ phosphor and (d) TL curves of $Sr_2LaGaO_5:0.06Eu^{2+}$ and Sr_2LaGaO_5 host; the illustration shows the afterglow generated by turning off the light source sample after 1 min irradiation with a 360 nm light source.

small values indicate that the refinement was reliable.[20] Tables S2 and S3 list the fractional atomic coordinates and primary bond lengths of Sr_2LaGaO_5:xEu.[20] As presented in Figure 1d, an increasing x(Eu) leads to the gradual reduction of the cell volume V, which could be attributed to the ion replacement of $Eu^{2+} \leftrightarrow Sr^{2+}$ because the ionic radius of Eu^{2+} is slightly smaller than that of Sr^{2+} (Eu^{2+}, (CN = 8, IR = 1.25 Å) (CN = 10, IR = 1.35 Å); Sr^{2+}, (CN = 8, IR = 1.26 Å) (CN = 10, IR = 1.36 Å)).[21,22] In addition, the substitution of $Eu^{3+} \leftrightarrow La^{3+}$ ions may also be another reason for the decrease in cell volume V after doping with Eu (Eu^{3+}, (CN = 8, IR = 1.066 Å); La^{3+}, (CN = 8, IR = 1.16 Å)). Besides, it is also possible for a small number of Eu^{2+} ions to occupy the La^{3+} site. The question of which sites Eu^{2+} is more likely to occupy will be further discussed later. A SEM image and element atlas image of $Sr_2LaGaO_5:0.06Eu^{2+}$ are shown in Figure 1e. The particle size of the sample is about 15−30 μm, and the shape is irregular, indicating that the microcrystals have a high-quality crystallinity. In addition, the element mapping images also show that Sr, La, Ga, O, and Eu were uniformly distributed in the phosphor particles.

Photoluminescence. Figure 2a demonstrates the luminescence behaviors of $Sr_2LaGaO_5:0.06Eu^{2+}$. Obviously, the luminescence intensity of the sample was significantly improved after secondary sintering. At the same time, monitoring the luminescence of Eu^{3+} under the excitation of 393 nm before and after secondary sintering indicates that the Eu^{3+} luminescence is significantly reduced after secondary sintering, which proves that more Eu^{3+} is reduced to Eu^{2+} (Figure S2). Through a comparison of the XRD patterns before and after secondary sintering, it can be seen that all samples belong to the pure phase (Figure S3). The photoluminescence excitation (PLE) spectrum of the sample was monitored at 618 nm, which exhibited a broadband spectrum from 380 to 600 nm attributed to $4f^7 \rightarrow 4f^6\ 5d^1$ transitions of Eu^{2+} ions.[23] Under 450 nm excitation, $Sr_2LaGaO_5:0.06Eu^{2+}$ exhibited a broadband emission from 550 to 800 nm, with a full width at half-maximum (fwhm) of 78.2 nm. As shown in Figure S4, all of the samples display similar peak positions and spectral profiles under 450 nm excitation, and x = 6% is the optimal doping concentration. In order to further understand the dynamics of the Eu^{2+} excited state in Sr_2LaGaO_5 and further confirm the site occupation of Eu^{2+}, we conducted temperature-dependent PL decay curve measurements in the temperature range from 78 to 330 K. The decay curves and the detailed fitting results are summarized in Figure 2b and Table S4, respectively. Obviously, all decay curves fitted well with the double exponential function $I(t) = A_1 e^{-t/\tau_1} + A_2 e^{-t/\tau_2}$, indicating that all samples have two luminescence centers. Generally, as the temperature decreases, the probability of non-radiative transitions decreases, and the emission attenuation gradually extends.[24] As can be seen, it is found that the Eu^{2+}-PL decay in Sr_2LaGaO_5 was significantly increased at 330 K compared with that at 78 K (Figure 2b, Table S4). The abnormal temperature decay of Eu^{2+} with increasing temperature can be explained by the capture of electrons thermally filled at the Eu^{2+} $5d$ level.

As shown in Figure 2c, $Sr_2LaGaO_5:Eu^{2+}$ exhibits a weak and brief afterglow decay after 450 nm excitation. The reason for the existence of this decay is related to the defects generated by Eu^{2+} occupation at the La^{3+} position. To confirm this speculation, we studied the distribution of $Sr_2LaGaO_5:Eu^{2+}$ traps through TL spectroscopy, as depicted in Figure 2d. Apparently, $Sr_2LaGaO_5:Eu^{2+}$ phosphors possess deep traps near 85 °C compared to the Sr_2LaGaO_5 host. Typically, delayed photoluminescence emerges in phosphors with traps, which corresponds to the PL decay curve (Figure 2b, Table S4).[25] Thus, one of the luminescence centers occupied by Eu^{2+} should be La^{3+}. Admittedly, the main factors affecting the emission energy distribution of Eu^{2+} are the nephelauxetic effect, crystal field splitting, and Stokes shift.[26,27] Dorenbos has

https://doi.org/10.1021/acs.chemmater.3c01980
Chem. Mater. 2023, 35, 8714−8721

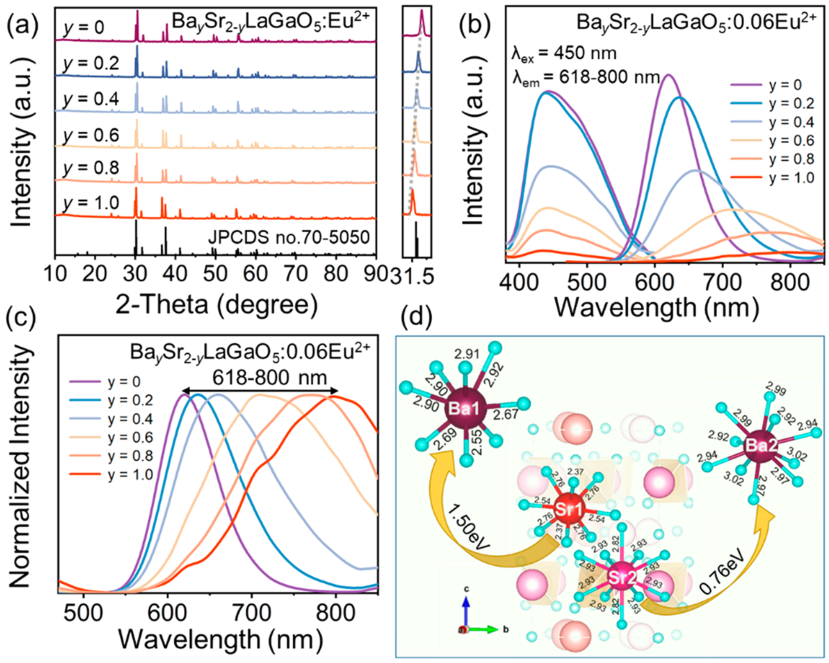

Figure 3. (a) XRD patterns of $Ba_ySr_{2-y}LaGaO_5$:0.06Eu^{2+} ($0 \leq y \leq 1$). (b) Photoluminescence emission and excitation spectra of $Ba_ySr_{2-y}LaGaO_5$:0.06Eu^{2+} ($0 \leq y \leq 1$). (c) Normalized emission spectra of $Ba_ySr_{2-y}LaGaO_5$:0.06Eu^{2+} ($0 \leq y \leq 1$) under 450 nm excitation. (d) The required formation energy model for Ba^{2+} to replace Sr^{2+} at different sites in the calculation model with the lowest formation energy.

studied the ε_{CFS} of Ce^{3+} in oxides, and the empirical formula for determining the relationship between the shape and volume of the coordination polyhedra and crystal field splitting is given as follows.[28]

$$\varepsilon_{cfs} = \beta_{poly}^{Q} R_{av}^{-2}$$

$$R_{av} = \frac{1}{N} \sum_{i=1}^{N} (R_i - 0.6\Delta R)$$

Among them, β_{poly}^{Q} is a constant that depends on the type of polyhedron and is independent of the valence state of rare earth ions. The optical properties of Ce^{3+} and Eu^{2+} are similar. R_i is the distance between the coordination anion and Eu^{2+} in a lattice without relaxation, and there are N coordination anions. However, due to the actual lattice relaxation around Eu^{2+}, 0.6ΔR is introduced to correct the distance between the atoms, $\Delta R = R_M - R_{Eu}$, where R_M is the ionic radius of the cation replaced by Eu^{2+} and R_{Eu} is the ionic radius of Eu^{2+}. In addition, Dorenbos summarized the following empirical equation through data statistics and analysis: $\beta_{Octahedron}$:$\beta_{Hexahedron}$:$\beta_{Cubic\ Octahedron}$ = 1:0.89:0.44. Accordingly, the coordination numbers of octahedrons, hexahedrons, and cubic octahedrons are 6, 8, and 12, respectively. Therefore, the smaller the coordination number, the larger the crystal field splitting, giving rise to the redshift of the PL spectra.[29] For instance, some previous reports propose that the red emission is mainly dominated by Eu^{2+} occupying low coordination positions, such as Sr_2ScAlO_5:Eu^{2+} (Sr^{2+}, (CN = 6));[30] $CaYGaO_4$:Eu^{2+} (Ca^{2+}, (CN = 6));[31] and so on. In addition, our group also found that Eu^{2+} occupies eight-coordinated Sr sites in $SrLaScO_4$:Eu^{2+}, producing red emission.[32,33] Therefore, it is also credible that Eu^{2+} occupies the La^{3+} and Sr^{2+} sites with coordination numbers of CN = 8 in Sr_2LaGaO_5:Eu^{2+}, which leads to red emission.

Furthermore, $Ba_ySr_{2-y}LaGaO_5$:Eu^{2+} ($0 \leq y \leq 1$) phosphors have been prepared through Sr/Ba substitution, and their XRD patterns are shown in Figure 3a. All diffraction peaks are consistent with the standard data for Sr_2LaGaO_5 (JCPDS No. 70-5050). As the Ba doping amounts increase, the diffraction peaks gradually shift toward a small diffraction angle direction, which can be attributed to lattice expansion caused by substituting the larger Ba^{2+} for the smaller Sr^{2+} in the same fold of coordination (Sr^{2+}, (CN = 8, IR = 1.26 Å) (CN = 10, IR = 1.36 Å), Ba^{2+}, (CN = 8, IR = 1.42 Å) (CN = 10, IR = 1.52 Å)). Figure S5 shows SEM images and EDS patterns of the selected $Ba_{0.2}Sr_{1.8}LaGaO_5$:Eu^{2+} sample. The sample size is approximately 20−40 μm. The EDS diagram declares uniform distributions of Ba, Sr, La, Ga, O, and Eu in the phosphors. Through Sr/Ba substitution, the emission spectra of the samples gradually red shift, with a maximum displacement of 800 nm. The PLE and PL spectra of $Ba_ySr_{2-y}LaGaO_5$:Eu^{2+} ($0 \leq y \leq 1$) are further depicted in Figure 3b. As the Ba doping concentration gradually increases, the emission spectra gradually shift to the deep red region, while the luminescence intensity of the sample also decreases little by little. The corresponding PLQY values are listed in Table S5, from 40.5% at $y = 0$ to 10.3% at $y = 1$, suggesting the decreasing trend. The normalized PL spectrum of $Ba_ySr_{2-y}LaGaO_5$:Eu^{2+} ($0 \leq y \leq 1$) is shown in Figure 3c.

Strikingly, the emission peak position of the sample shifts from 618 to 800 nm (under 450 nm excitation). Moreover, the fwhm values of the spectra also exhibit significant broadening as the Ba doping amounts increase. Consequently, it can be further confirmed that the local structure of Eu^{2+} can be adjusted through Sr/Ba cation substitution, enabling spectral regulation of $Ba_ySr_{2-y}LaGaO_5$:Eu^{2+} ($0 \leq y \leq 1$) from the visible light (VIS) to near-infrared light (NIR) region. In view of the presence of two Sr sites (CN = 8 and CN = 10) in Sr_2LaGaO_5:Eu^{2+}, DFT calculations were used to determine which position of Sr is more easily replaced by Ba during the

https://doi.org/10.1021/acs.chemmater.3c01980
Chem. Mater. 2023, 35, 8714−8721

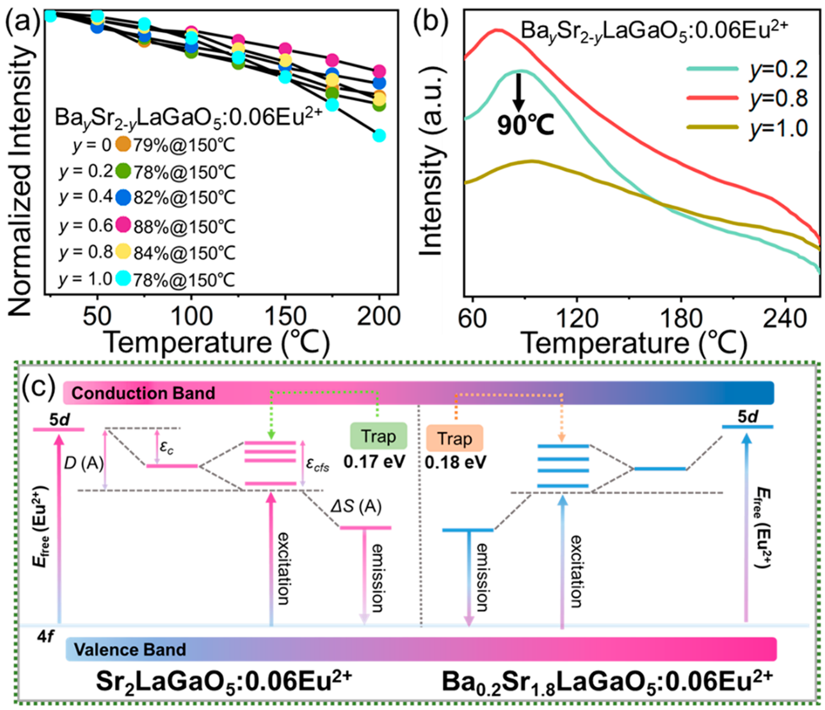

Figure 4. (a) Temperature-dependent normalized integrated emission intensities of $Ba_ySr_{2-y}LaGaO_5$:0.06Eu^{2+} ($0 \leq y \leq 1$) from room temperature to 200 °C under 450 nm excitation. (b) TL curves of $Ba_ySr_{2-y}LaGaO_5$:0.06Eu^{2+} ($0 \leq y \leq 1$) and (c) schematic energy level diagram for Eu^{2+} ions in Sr_2LaGaO_5 and $Ba_{0.2}Sr_{1.8}LaGaO_5$. ε_c denotes the centroid shift of 5*d*-levels of Eu^{2+}, ε_{cfs} shows the CFS effect, Efree represents the photoionization barrier, and $\Delta S(A)$ represents the Stokes shift.

substitution process. First, based on the structural prototype of Sr_2LaGaO_5,[19] various structural models were constructed for theoretical calculations by randomly fixing the positions of Sr1 and La, as shown in Figure S6. La atom replaced the Sr site that is eight-coordinated to the O atom to form [LaO_8]. All [LaO_8] exists between the [SrO_{10}] and [GaO_4] layers. Note that all the La is fixed with the ratio of Sr:La = 2:1. Therefore, the Ba/Sr replacement models were constructed by using the structure with the lowest formation energy as shown in the calculation results, and the model with the lowest energy is labeled in blue (Figure S6, iii). Based on this model, the final calculation results indicate that Ba tends to replace the Sr2 site with the formation energy of 0.76 eV to form a ten-coordinated [BaO_{10}] rather than that of the Sr1 site (1.50 eV) to create an eight-coordinated [BaO_8]. Since the ionic radius (IR) of Ba^{2+} (CN = 10, IR = 1.52 Å) is larger than that of Sr^{2+} (CN = 10, IR = 1.36 Å), the introduction of Ba ions will cause the expansion of the ten-coordinated [Sr/BaO_{10}] polyhedron and generate compressive stress around the eight-coordinated [Sr1/Eu1O_8] and [La/Eu2O_8], resulting in structural distortion (Figure 3d and Figure S6). Distinct Stokes displacement caused by sizable structural relaxation contributes significantly to the enormous PL displacement.[34] Therefore, we speculate that the red shift and broadening of the spectrum are caused by the Octahedron distortion of [Eu1O_8] and [Eu2O_8].

Figure 4a and Figure S7 show the temperature-dependent emission spectra of $Ba_ySr_{2-y}LaGaO_5$:Eu^{2+} ($0 \leq y \leq 1$) phosphors under 450 nm excitation. Due to the different sensitivity responses of Eu^{2+} to La and Sr1 sites at different temperatures, the temperature-dependent PL peaks of all samples exhibit a slight blue shift, as shown in Figure S7. Moreover, all samples indicate good thermal stability, with a comprehensive emission intensity of approximately 78%−88% at 150 °C compared to the initial value at RT. In addition, the thermal stability of this material compared to other typical red phosphors is also listed (Table S6). Figure 4b shows the TL spectra of $Ba_ySr_{2-y}LaGaO_5$:Eu^{2+} ($0 \leq y \leq 1$). The principle of this temperature-dependent spectral phenomenon was further studied through the trap distribution. All samples contain defects, and different trap depths lead to slight differences in the thermal stability. However, the introduction of Ba did not increase the number of traps in the samples. Taking Sr_2LaGaO_5:Eu^{2+} and $Ba_{0.4}Sr_{1.6}LaGaO_5$:Eu^{2+} as examples, the trap depths of the two samples were estimated using the corresponding formulas:[35]

$$E_T = \frac{T}{500}\ \text{eV}$$

In the equation, E_T represents the estimated depth in eV and T represents the peak temperature in kelvin (K). At 85 and 90 °C, the E_T values are 0.17 and 0.18 eV, respectively. A visualization mechanism model on the PL and carrier compensation diagram was created to compare the effects of defects before and after Ba doping, as shown in Figure 4c. Under 450 nm excitation, the electrons on the Eu^{2+} level rise to the 5*d* excited state, and red emission will be achieved when the excited electrons return to the 4*f* ground state. However, when there are defects in the sample, a portion of the electrons will be trapped and escape, thereby improving the thermal stable emissions of the samples. Moreover, due to the introduction of Ba, no new traps are generated, so the thermal stability of all samples remains relatively stable. As mentioned earlier, phosphors with traps generally exhibit delayed photoluminescence, which may affect the PL decay curve. Figure S8 and Table S7 show the temperature-dependent PL

https://doi.org/10.1021/acs.chemmater.3c01980
Chem. Mater. 2023, 35, 8714−8721

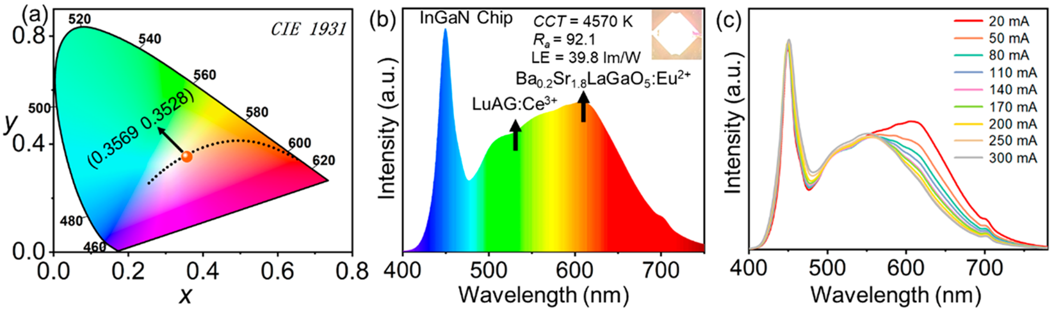

Figure 5. (a) CIE chromaticity coordinates of WLED and the device fabricated by blending green-emitting $LuAG:Ce^{3+}$ and red-emitting $Ba_{0.2}Sr_{1.8}LaGaO_5:Eu^{2+}$ phosphors based on an InGaN blue-emitting (λ_{em} = 450 nm) chip. (b) PL spectra of the WLED device and the WLED lamp are excited in the inset. (c) PL spectra of the fabricated WLED under 20−300 mA forward bias currents.

decay in the temperature at 80 and 300 K of $Ba_{0.4}Sr_{1.6}LaGaO_5:Eu^{2+}$. Notably, its changes are consistent with Figure 2b and Table S4, so this will not be further elaborated.

WLED devices were fabricated by coating commercial green-emitting $LuAG:Ce^{3+}$ and red-emitting $Ba_{0.2}Sr_{1.8}LaGaO_5:Eu^{2+}$ on the commercial 450 nm LED chips to evaluate their potential lighting source applications. As shown in Figure 5a, the International Commission on I'Eclairage (CIE) coordinates of the WLED manufactured are (0.357, 0.353). Figure 5b shows the output spectrum of the device under a forward bias current of 20 mA. The CCT is determined to be 4570 K, located in the white light area, and R_a is 92.1. The illustration shows a photo of the glowing WLED with shinning white light. The output spectra of the WLED device at a driving current of 20−300 mA are shown in Figure 5c. These results on the WLED device indicate that the $Ba_{0.2}Sr_{1.8}LaGaO_5:Eu^{2+}$ phosphor is a potential red converter for capturing warm white light.

■ CONCLUSIONS

In conclusion, we have demonstrated that Eu^{2+} occupying the eight-coordinated [$Sr1/LaO_8$] sites in Sr_2LaGaO_5 can be developed as a useful design principle toward red phosphors for warm white lighting sources. Moreover, giant photoluminescence tuning can be achieved through a simple Ba−Sr substitution in $Sr_2LaGaO_5:Eu^{2+}$. It is found that Ba is more inclined to selectively replace the ten-coordinated [$Sr2O_{10}$] sites, resulting in a strong CFS and compression of [$Eu1O_8$] and [$Eu2O_8$] polyhedra, enabling a spectral shift from visible to near-infrared. Moreover, $Ba_ySr_{2-y}LaGaO_5:Eu^{2+}$ ($0 \leq y \leq 1$) phosphors showed excellent thermal quenching resistance, attributed to the existence of defect levels. This also provides feasible guidance for developing Eu^{2+} doped oxide-based near-infrared luminescent phosphors. A WLED with high color index (R_a = 92.1) was fabricated by combining $Ba_{0.2}Sr_{1.8}LaGaO_5:Eu^{2+}$ with a blue chip and green-emitting phosphors $LuAG:Ce^{3+}$. This work demonstrated some new design principles toward Eu^{2+} activated oxide-based red phosphors as well as achieving tunable emission through cations' substitution.

■ ASSOCIATED CONTENT

Supporting Information

The Supporting Information is available free of charge at https://pubs.acs.org/doi/10.1021/acs.chemmater.3c01980.

Tables S1−S6 and Figures S1−S6 showing additional PXRD patterns, X-ray refinement, PLQYs, additional PL and PL decay spectra, calculated structural models, and temperature-dependent emission spectra of the studied samples (PDF)

■ AUTHOR INFORMATION

Corresponding Author

Zhiguo Xia − *The State Key Laboratory of Luminescent Materials and Devices, Guangdong Provincial Key Laboratory of Fiber Laser Materials and Applied Techniques, Guangdong Engineering Technology Research and Development Center of Special Optical Fiber Materials and Devices, School of Materials Science and Engineering, South China University of Technology, Guangzhou 510641, P. R. China;* orcid.org/0000-0002-9670-3223; Email: xiazg@scut.edu.cn

Authors

Yu Chen − *The State Key Laboratory of Luminescent Materials and Devices, Guangdong Provincial Key Laboratory of Fiber Laser Materials and Applied Techniques, Guangdong Engineering Technology Research and Development Center of Special Optical Fiber Materials and Devices, School of Materials Science and Engineering, South China University of Technology, Guangzhou 510641, P. R. China*

Zhiyu Yang − *Department of Mathematics and Physics, Chongqing University of Posts and Telecommunications, Chongqing 400065, China*

Jiance Jin − *The State Key Laboratory of Luminescent Materials and Devices, Guangdong Provincial Key Laboratory of Fiber Laser Materials and Applied Techniques, Guangdong Engineering Technology Research and Development Center of Special Optical Fiber Materials and Devices, School of Materials Science and Engineering, South China University of Technology, Guangzhou 510641, P. R. China;* orcid.org/0000-0002-4876-2018

Jianwei Qiao − *College of Physics, Taiyuan University of Technology, 030024 Taiyuan, China*

Yuzhen Wang − *The State Key Laboratory of Luminescent Materials and Devices, Guangdong Provincial Key Laboratory of Fiber Laser Materials and Applied Techniques, Guangdong Engineering Technology Research and Development Center of Special Optical Fiber Materials and Devices, School of Materials Science and Engineering, South China University of Technology, Guangzhou 510641, P. R. China*

https://doi.org/10.1021/acs.chemmater.3c01980
Chem. Mater. 2023, 35, 8714−8721

Maxim S. Molokeev − *Laboratory of Crystal Physics, Kirensky Institute of Physics, Federal Research Center KSC SB RAS, Krasnoyarsk 660036, Russia; World-Class Research Center "Advanced Digital Technologies", University of Tyumen, Tyumen 625003, Russia;* orcid.org/0000-0002-8297-0945

Hendrik C. Swart − *Department of Physics, University of the Free State, Bloemfontein ZA-9300, South Africa;* orcid.org/0000-0001-5233-0130

Complete contact information is available at:
https://pubs.acs.org/10.1021/acs.chemmater.3c01980

Notes

The authors declare no competing financial interest.

■ ACKNOWLEDGMENTS

This research was supported by the National Key Research and Development Program of China (2021YFB3500401 and 2021YFE0105700), the National Natural Science Foundations of China (Grant Nos. 51972118 and 52102169), the Local Innovative and Research Teams Project of Guangdong Pearl River Talents Program (2017BT01X137), the China Postdoctoral Science Foundation (2021M691053), and the Young Elite Scientists Sponsorship Program by China Association for Science and Technology (No. YESS20200053). This work was also supported by the Ministry of Science and Higher Education of the Russian Federation as part of World-class Research Center program: "Advanced Digital Technologies", contract no. 075-15-2022-314.

■ REFERENCES

(1) Qiao, J.; Ning, L.; Molokeev, M. S.; Chuang, Y. C.; Liu, Q.; Xia, Z. Eu^{2+} Site Preferences in the Mixed Cation $K_2BaCa(PO_4)_2$ and Thermally Stable Luminescence. *J. Am. Chem. Soc.* **2018**, *140*, 9730−9736.

(2) Qiao, J.; Zhang, S.; Zhou, X.; Chen, W.; Gautier, R.; Xia, Z. Near-Infrared Light-Emitting Diodes utilizing a Europium-Activated Calcium Oxide Phosphor with External Quantum Efficiency of up to 54.7%. *Adv. Mater.* **2022**, *34*, 2201887.

(3) Qin, X.; Liu, X.; Huang, W.; Bettinelli, M.; Liu, X. Lanthanide-Activated Phosphors Based on 4*f*-5*d* Optical Transitions: Theoretical and Experimental Aspects. *Chem. Rev.* **2017**, *117*, 4488−4527.

(4) Li, Z.; Zhao, X.; Jiang, Y. Hydrothermal Preparation and Photoluminescent Property of $LiY(MoO_4)_2$:Pr^{3+} Red Phosphors for White Light-Emitting Diodes. *J. Rare Earth.* **2015**, *33*, 33−36.

(5) Teng, X.; Liu, Y.; Liu, Y.; Hu, Y.; He, H.; Zhuang, W. Preparation and Luminescence Properties of the Red-Emitting Phosphor $(Sr_{1-x}Ca_x)_2Si_5N_8$:Eu^{2+} with Different Sr/Ca Ratios. *J. Rare Earth.* **2009**, *27*, 58−61.

(6) Guan, L.; Wang, Y.; Chen, W.; Jin, L.; Li, X.; Guo, Q.; Yang, Z.; Fu, G. Fabrication and Luminescent Properties of Red Phosphor M_3BO_6:Eu^{3+}(M = La, Y). *J. Rare Earth.* **2010**, *28*, 295−298.

(7) Cai, C.; Qian, J.; Zhang, B.; Hu, W.; Hao, L.; Xu, X.; Wang, Y. Synthesis of Red-Emitting $CaAlSiN_3$:Eu^{2+} Phosphors Through a Cost-effective Synthetic Route. *ECS J. Solid State Sci. Technol.* **2014**, *3*, R169−R172.

(8) Pust, P.; Weiler, V.; Hecht, C.; Tucks, A.; Wochnik, A. S.; Henss, A. K.; Wiechert, D.; Scheu, C.; Schmidt, P. J.; Schnick, W. Narrow-band Red-Emitting $Sr[LiAl_3N_4]$:Eu^{2+} as A Next-generation LED-phosphor Material. *Nat. Mater.* **2014**, *13*, 891−896.

(9) Guo, C.; Huang, D.; Su, Q. Methods to Improve the Fluorescence Intensity of CaS:Eu^{2+} Red-Emitting Phosphor for White LED. *Mater. Sci. Eng., B* **2006**, *130*, 189−193.

(10) Takahashi, T.; Adachi, S. Mn^{4+}-Activated Red Photoluminescence in K_2SiF_6 Phosphor. *J. Electrochem. Soc.* **2008**, *155*, E183−E188.

(11) Zhu, H.; Lin, C. C.; Luo, W.; Shu, S.; Liu, Z.; Liu, Y.; Kong, J.; Ma, E.; Cao, Y.; Liu, R. S.; Chen, X. Highly Efficient Non-Rare-Earth Red Emitting Phosphor for Warm White Light-emitting Diodes. *Nat. Commun.* **2014**, *5*, 4312.

(12) Qiao, J.; Ning, L.; Molokeev, M. S.; Chuang, Y. C.; Zhang, Q.; Poeppelmeier, K. R.; Xia, Z. Site-Selective Occupancy of Eu^{2+} Toward Blue-Light-Excited Red Emission in a $Rb_3YSi_2O_7$: Eu Phosphor. *Angew.Chem.Int.Ed.* **2019**, *58*, 11521−11526.

(13) Sato, Y.; Kuwahara, H.; Kato, H.; Kobayashi, M.; Masaki, T.; Kakihana, M. Large Redshifts in Emission and Excitation from Eu^{2+}-Activated Sr_2SiO_4 and Ba_2SiO_4 Phosphors Induced by Controlling Eu^{2+} Occupancy on the Basis on Crystal-Site Engineering. *Opt. Photonics J.* **2015**, *05*, 326−333.

(14) Yang, Z.; Zhao, Y.; Zhou, Y.; Qiao, J.; Chuang, Y. C.; Molokeev, M. S.; Xia, Z. Giant Red-Shifted Emission in (Sr,Ba)-Y_2O_4:Eu^{2+}Phosphor Toward Broadband Near-Infrared Luminescence. *Adv. Funct. Mater.* **2022**, *32*, 2103927.

(15) Kresse, G.; Joubert, D. From Ultrasoft Pseudopotentials to The Projector Augmented-Wave Method. *Phys. Rev. B* **1999**, *59*, 1758−1775.

(16) Kresse, G.; Furthmüller, J. Efficient Iterative Schemes for Ab Initio Total-Energy Calculations Using A Plane-Wave Basis Set. *Phys. Rev. B, Condens Matter.* **1996**, *54*, 11169−11186.

(17) Blöchl, P. E. Projector Augmented-Wave Method. *Phys. Rev. B* **1994**, *50*, 17953.

(18) Perdew, J. P.; Burke, K.; Ernzerhof, M. Generalized Gradient Approximation Made Simple. *Phys. Rev. Lett.* **1996**, *77*, 3865−3868.

(19) Gesing, T. M.; Uecker, R.; Buhl, J.-C. Crystal structure of distrontium lanthanum gallium pentaoxide, Sr_2LaGaO_5. *Z. Krist-New. Cryst. St.* **2000**, *215*, 317.

(20) Bruker, AXS, K. *Bruker AXS TOPAS V4: General profile and structure analysis software for powder diffraction data. - User's Manual*; Bruker AXS: Karlsruhe, Germany, 2008.

(21) Ahrens, L. H. The Use of Ionization Potentials Part 1. Ionic Radii of The Elements. *Geochim. Cosmochim. Acta* **1952**, *2*, 155−169.

(22) Coulson, C. *Pauling's Chemical Bond*; Springer: 1961.

(23) Chen, M.; Xia, Z.; Molokeev, M. S.; Lin, C. C.; Su, C.; Chuang, Y.-C.; Liu, Q. Probing Eu^{2+} Luminescence from Different Crystallographic Sites in $Ca_{10}M(PO_4)_7$:Eu^{2+} (M = Li, Na, and K) with β-$Ca_3(PO_4)^{2-}$ Type Structure. *Chem. Mater.* **2017**, *29*, 7563−7570.

(24) Hu, T.; Gao, Y.; Molokeev, M. S.; Xia, Z.; Zhang, Q. Eu^{2+} Stabilized at Octahedrally Coordinated Ln^{3+} Site Enabling Red Emission in $Sr_3LnAl_2O_{7.5}$ (Ln = Y or Lu) Phosphors. *Adv. Opt. Mater.* **2021**, *9*, 2100077.

(25) Yang, Z.; Zhou, Y.; Qiao, J.; Molokeev, M. S.; Xia, Z. Rapid Synthesis of Red-Emitting $Sr_2Sc_{0.5}Ga_{1.5}O_5$:Eu^{2+} Phosphors and the Tunable Photoluminescence Via Sr/Ba Substitution. *Adv. Opt. Mater.* **2021**, *9*, 2100131.

(26) Dorenbos, P. f → d Transition Energies of Divalent Lanthanides In Inorganic Compounds. *J. Phys.: Condens. Matter* **2003**, *15*, 575−594.

(27) Wang, S.; Song, Z.; Kong, Y.; Liu, Q. Relationship of Stokes Shift with Composition and Structure in Ce^{3+}/Eu^{2+}-Doped Inorganic Compounds. *J. Lumin.* **2019**, *212*, 250−263.

(28) Dorenbos, P. Crystal Field Splitting of Lanthanide $4f^{n-1}5d$-Levels in Inorganic Compounds. *J. Alloys Compd.* **2002**, *341*, 156−159.

(29) Dorenbos, P. A Review on How Lanthanide Impurity Levels Change with Chemistry and Structure of Inorganic Compounds. *ECS J. Solid. State. Sci. Technol.* **2013**, *2*, R3001−R3011.

(30) Zhou, T.; Song, Z.; Song, X.; Bian, L.; Liu, Q. A Red Oxide Phosphor, Sr_2ScAlO_5:Eu^{2+} with Perovskite-Type Structure, for White Light-Emitting Diodes. *Chin. Phys. B* **2010**, *19*, 127808.

(31) Hu, T.; Jiang, Z.; Wang, B.; Yu, T.; Wen, D.; Zeng, Q.; Gao, Y. Eu^{2+} Luminescence in $CaYGaO_4$ Olivine: a New Efficient Red

Phosphor for Warm Illumination. *J. Mater. Chem. C* **2023**, *11*, 2153−2161.
(32) Yang, Z.; Liu, G.; Zhao, Y.; Zhou, Y.; Qiao, J.; Molokeev, M. S.; Swart, H. C.; Xia, Z. Competitive Site Occupation toward Improved Quantum Efficiency of $SrLaScO_4$:Eu Red Phosphors for Warm White LEDs. *Adv. Opt. Mater.* **2022**, *10*, 2102373.
(33) Yang, Z.; Zhao, Y.; Ueda, J.; Molokeev, M. S.; Shang, M.; Xia, Z. Engineering Charge-Transfer Interactions for Red-Emitting $SrLa(Sc,Ga)O_4$:Ce^{3+} Phosphor with Improved Thermal Stability. *Sci. China Mater.* **2023**, *66*, 1989−1996.
(34) Phung, Q. M.; Barandiarán, Z.; Seijo, L. Structural Relaxation Effects on The Lowest 4*f*-5*d* Transition of Ce^{3+} in garnets. *Theor. Chem. Acc.* **2015**, *134*, 141−149.
(35) Xiong, P.; Peng, M.; Qin, K.; Xu, F.; Xu, X. Visible to Near-Infrared Persistent Luminescence and Mechanoluminescence from Pr^{3+}-Doped $LiGa_5O_8$ for Energy Storage and Bioimaging. *Adv. Opt. Mater.* **2019**, *7*, 1901107.

https://doi.org/10.1021/acs.chemmater.3c01980
Chem. Mater. 2023, 35, 8714−8721